

# ENAS U-Net: Evolutionary Neural Architecture Search for Retinal Vessel Segmentation

Zhun Fan<sup>1,2</sup>, *Senior Member, IEEE*, Jiahong Wei<sup>1,2</sup>, Guijie Zhu<sup>1,2</sup>, Jiajie Mo<sup>1,2</sup>, and Wenji Li<sup>1,2</sup>

<sup>1</sup>Department of Electronic and Information Engineering, Shantou University, Shantou 515063, China

<sup>2</sup>Key Lab of Digital Signal and Image Processing of Guangdong Province, Shantou University, Shantou 515063, China

zfan@stu.edu.cn; 19jhwei@stu.edu.cn; 16gjzhu@stu.edu.cn; jiajiemo@outlook.com; liwj@stu.edu.cn

## Abstract:

The accurate retina vessel segmentation (RVS) is of great significance to assist doctors in the diagnosis of ophthalmology diseases and other systemic diseases, and manually designing a valid neural network architecture for retinal vessel segmentation requires high expertise and a large workload. In order to further improve the performance of vessel segmentation and reduce the workload of manually designing neural network. We propose a specific search space based on encoder-decoder framework and apply neural architecture search (NAS) to retinal vessel segmentation. The search space is a macro-architecture search that involves some operations and adjustments to the entire network topology. For the architecture optimization, we adopt the modified evolutionary strategy which can evolve with limited computing resource to evolve the architectures. During the evolution, we select the elite architectures for the next generation evolution based on their performances. After the evolution, the searched model is evaluated on three mainstream datasets, namely DRIVE, STARE and CHASE\_DB1. The searched model achieves top performance on all three datasets with fewer parameters (about 2.3M). Moreover, the results of cross-training between above three datasets show that the searched model is with considerable scalability, which indicates that the searched model is with potential for clinical disease diagnosis.

**Key Words:** Neural Architecture Search; Retinal Vessel Segmentation; Evolutionary Strategy; Convolutional Neural Network

## 1. Introduction

Retinal vessel segmentation has always been valued by researchers in the field of medical image processing, because the pathological changes of retinal blood vessels can reflect either ophthalmology diseases or other systemic diseases, such as high blood pressure, diabetes, arteriolosclerosis. At present, ophthalmologists and other doctors would consider the fundus examination as a routine clinical examination [56]. At the same time, the fundus vascular system is the only human blood vascular system that can be observed in vivo [57][58]. Through the observation of the fundus vascular system can be a considerable diagnosis and tracking of many diseases [57]. Retinal vessel segmentation is also a prerequisite step for quantitative analysis of fundus images. Through the retinal vessel segmentation, the relevant morphological information of retinal vascular tree (such as the width, length and curvature of blood vessels, etc.) can be obtained [31]. Meanwhile, the vascular tree of retinal vessels has unique characteristics and can also be applied to biometrics [59][60]. So accurate segmentation of retinal vessels is of great significance.

The structure of the retinal vasculature tree is very complicated, with lots of interconnected and

closely connected blood vessels, but also many tiny and weak blood vessels. And the difference between the vascular region and the background is subtle. Additionally, fundus images are susceptible to noise and uneven illumination. As indicated above, it is very challenging to segment the retinal vascular tree from fundus images. Although many manually designed neural network architectures for retinal vessel segmentation have been proposed, there are some limitations of these models. The existing neural network models are still difficult to capture vascular tree under complicated situation of fundus images. In this case, it is necessary to design a neural network model with fine architecture to extract the features of the complicated vascular tree more accurately. At present, the neural network architectures are designed manually, which requires high quality skilled expertise, requires repeated trial and error experiments, and has weaknesses such as strong subjectivity, high labor intensity and low efficiency.

In recent years, the research on neural architecture search (NAS) has been very popular. NAS can design the architecture automatically, and can also lead to new neural network architectures with better performance. Similarly, according to the characteristics of neural network architecture obtained by NAS, empirical information can be summarized to guide us to better manually design neural network architecture.

In this paper, we apply neural architecture search (NAS) with an evolutionary algorithm as optimization method to retinal vessel segmentation. In order to better improve the performance of RVS and automatically search a neural network architecture, we propose a specific search space based on encoder-decoder framework inspired by U-Net[2]. For macro-architecture search, we also adopt an encoding method with fixed length and non-redundant binary code to represent the neural network architecture and use modified evolutionary strategy (ES) to search efficiently under the large search space. ES can evolve with fewer individuals of the population compared with other evolutionary algorithms for constraints of limited computing resources. As shown in Figure 1, during the architecture evolution, we adopt standard operations of evolutionary strategy (ES) (e.g. selection and mutation) to produce more competitive neural network architectures, and the survival of the fittest based on the performances of the architectures. When evaluating the performances of the architectures, the model would be trained independently and assign F1-score in RVS as the fitness of each individual. Our specific contributions are as follows:

- It is the first time that NAS is applied to retinal vessel segmentation.
- We propose a specific search space based on encoder-decoder framework, and use modified evolutionary strategy to automatically optimize the neural network architecture in this search space, and automatically find out a more suitable neural network architecture for retinal vessel segmentation.
- The searched model achieves the top performance on three public available datasets, DRIVE [13], STARE [14], CHASE\_DB1 [39]. Meanwhile, cross-training between these three datasets verify the robustness and scalability of the searched model.

The remainder of this paper is structured as follows: Section 2 reviews related work with a focus on retinal vessel segmentation and neural architecture search. Section 3 introduces the proposed method. Section 4 presents the evaluation metrics, loss function and datasets. Section 5 describes the result of architecture evolution and experimental results of the searched model. Finally, we conclude this work in Section 6.

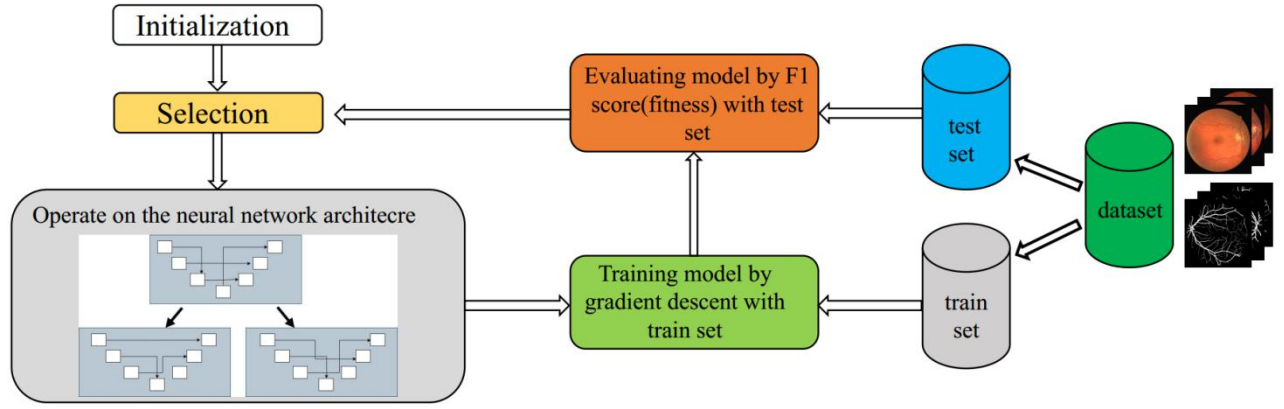


Figure 1. Overview of our method. Our approach is an architecture search process based on evolutionary strategy. the model is trained on a retina vessel dataset and assigned F1-score of the trained model as the fitness. The evolution strategy will search for better architectures.

## 2. Related work

### 2.1 Retinal vessel segmentation

Since FCN[1] and U-Net[2] were proposed, image segmentation methods based on full convolutional neural networks have become mainstream because of their excellent effects. Retinal vessel segmentation is a subclass of image segmentation. Recently, the new state-of-the-art methods [55][54][31][30][29][40] for retinal vessel segmentation are dominated by lots of neural network models, especially variants of U-Net.

[55] adopts a joint-loss to train the U-Net model. Two branches are responsible for pixel-wise loss and segment-level loss, respectively. The joint-loss could promote the model to balance the importance between thick and thin vessels. [54] adds pretrained components of MobileNetV2 [61] as the encoder and introduces novel contractive bottleneck blocks as the decoder, which achieve better performance and faster inference speed. [31] replaces traditional convolution with deformable convolution into U-Net to capture the miscellaneous morphology of vascular trees. [40] includes dense dilated convolutional block between the same stage encoder cell and decoder cell of the U-Net, and also uses a regularized walk algorithm to post-process model prediction. [29] designs a novel inception-residual block and introduce four supervision paths with different kernel size of convolution to utilize multi-scale features. The model in [30] has two encoders based on U-Net. One encoder path is for extracting spatial information and the other path is for extracting context information. Also, a novel module is used to combine the information of two paths. All the above methods which are mainly to adjust the architecture of neural network achieve a well performance for retinal vessel segmentation. This reflects the importance of neural network architecture for retinal vessel segmentation.

### 2.2 Neural architecture search

Depending on the search method, NAS can be divided into three types: reinforcement learning based, evolutionary algorithm based and differential architecture search. The method based on reinforcement learning [42][43][44] is to sample the neural network architectures and use a controller to learn how to generate better architectures from continual trial and error, with the performance of the models as reward feedback to the controller. The method based on evolutionary algorithms [11][12] is to perform operations on the neural network architecture (such as crossover and mutation) to generate off-springs, and to continuously adjust the neural network architectures from generation to generation

according to the law of survival of the fittest, and finally obtain the optimized model. For differential neural architecture search [45][46], each operation of the cell is assigned a weight coefficient. The parameter weight of neural network and the weight of each operation are updated alternately by gradient descent. The optimal model can be obtained by selecting the operation with the largest weight after convergence.

After the successes of NAS in image recognition, some researchers have also extended NAS to image segmentation [4] and object detection [47][48]. Similarly, there are also some works applying NAS to medical image segmentation. [49], [50] and [51] are mainly to optimize the hyperparameters and operations of each layer of the neural network. [52] and [53] belong to cell-based method that optimizes the structure and operations inside the cell based on U-Net. Moreover, there is no work applying NAS to retinal vessel segmentation.

### **3. Proposed method**

In this section, we will focus on how to use NAS for RVS and the optimization method of neural network architecture. As to improve the effect of RVS by a novel neural network architecture, it is necessary to specify the search space in the NAS process. In addition, because the evolutionary algorithm is used to automatically design the architecture of the neural network, the representation of the neural network architecture for evolving is equally important.

#### **3.1 Search Space**

##### **3.1.1 Basic Framework of the Network Architecture**

Since FCN[1] and original U-Net[2] with skip connections added for better feature fusion, full convolutional neural networks with encoder-decoder structure are currently mainstream in image segmentation. Due to the outstanding performance of original U-Net and its brilliant transferability, the U-like neural network architectures (variations of original U-Net) are still the best choice in medical image segmentation. The architecture of the U-like neural network is mainly composed of encoder for down-sampling and decoder for up-sampling. The encoder will extract image features of different scales, and the decoder will recover the abstract features in the encoder to the original image size and classify each pixel in the original image. With the above consideration, the basic framework of the neural network architecture in our method is also a U-like architecture with several different cells. It mainly contains one initial-conv cell, three encoder cells, and three decoder cells, which means three down-sampling and three up-sampling. Figure 6 shows our final neural network architecture, and we can understand the basic framework of search space from this figure.

##### **3.1.2 Search Space for the Cells**

In many NAS methods, cell-based micro-search methods are mainly used, which is mainly a search of operations inside the cell, and the searched neural network architecture is mainly formed by stacking several of these cells with the same operation. Our method will search the internal operation of cells and skip connections between different cells, which is a macro search method different from cell-based micro search. Inspired by the [3], our method also includes several cells. Each cell would contain different operations. As shown in Table 1 and Figure 2, the search space of our method mainly includes the normalization methods, the activation functions, the up-sampling methods and the down-sampling methods, the shortcut connections inside the cells, and the skip connections with the preceding cells. At the same time, unlike Original U-Net, which uses fixed skip connections for feature fusion between cells, our method will search the skip connections between the cells to find a better feature fusion network architecture. In addition to the existence of skip connections between

different cells, the search space also contains the operation of whether to use the shortcut connection inside the cell. The work of paper [37][38] is to adjust the structure of the model based on connections, which have proved that these connections can make the model better carry out feature fusion and gradient back propagation, and improve the training effect of neural network model.

**Table 1. The proposed search spaces**

Operation	Search space	Feasible cell
Activation function	ReLU[7], SELU[8]	All cells
Normalization	Batch normalization[9], Instance normalization[10] or no normalization	All cells
Down-sampling	Max pooling, Average pooling	Encoder cells
Up-sampling	Bilinear interpolation, Transpose convolution	Decoder cells
Shortcut connection	Yes / No	Encoder cells, Decoder cells
Skip connection	Connections with preceding cells	Encoder cells, Decoder cells

We only use  $3 \times 3$  convolution, because [6] indicates that the  $5 \times 5$  convolution can be replaced by multilayer  $3 \times 3$  convolution to achieve larger receptive fields and reduce the parameters of the neural network, though some works[4][5] think that the  $5 \times 5$  convolution and larger receptive fields should be considered. The search space also contains some commonly used activation functions, normalization methods, and sampling methods. The number of convolution kernels in all cells is set to 128. When there are skip connections between different cells, if there is a dimension mismatch, we use  $1 \times 1$  convolution to adjust the channel number of feature map from preceding cells or resize the feature map by nearest neighbor interpolation.

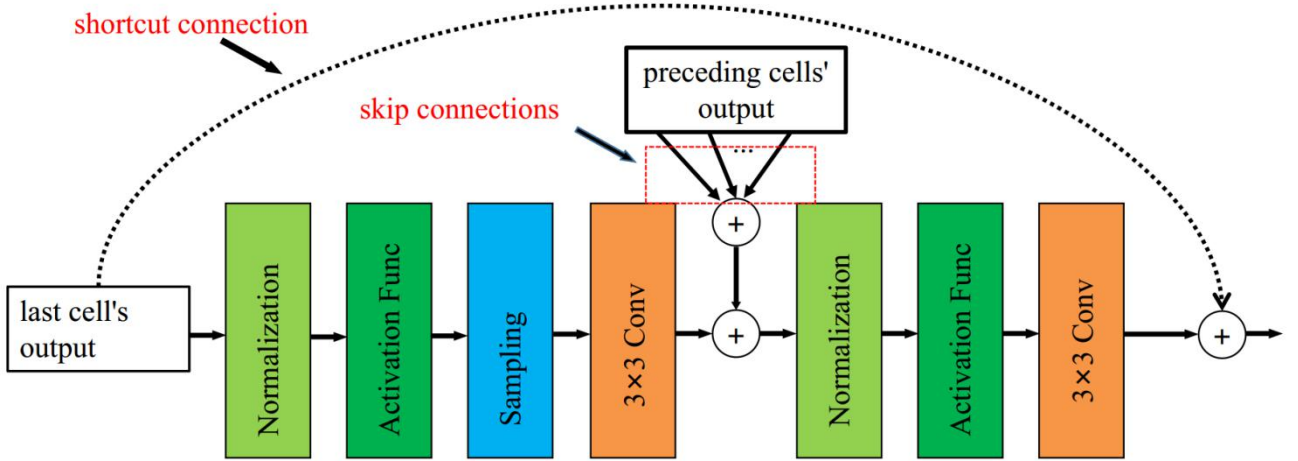


Figure 2. The proposed search space of the cells (There isn't shortcut connection, up-sampling and down-sampling in initial-conv cell. The difference between encoder cell and decoder cell is mainly reflected in up-sampling and down-sampling.)

### 3.2 Representation of the neural network architecture

Our method uses evolutionary algorithms to search network architectures for RVS, but generally does not directly operate on phenotypes. It operates on genotypes to affect phenotypes. Therefore, we need to introduce a reasonable way to encode the neural network architecture. Similar to [11][12], our method also adopts the binary bit to encode the network architecture. In order to search the architecture more efficiently, the coding of the architecture should be as short as possible, and there should be a one-to-one correspondence between genotype and phenotype. As shown in Figure 3, we

use a tuple  $(S, N_1, N_2, A, SC, SK_1, \dots, SK_i)$  with binary values to represent each cell, and each bit represents the corresponding operation.

- $S$  stands for sampling method of the corresponding cell. Max pooling or Average pooling for encoder cells, and bilinear interpolation or transpose convolution for decoder cells.
- $N_1$  indicates whether to use normalization.
- $N_2$  indicates which type of normalization, batch normalization or instance normalization.
- $A$  is a bit indicating which type of activation function would be used, ReLU or SELU.
- $SC$  indicates the in-cell shortcut connection.
- $SK_i$  means whether to take a skip connection with  $i^{th}$  cell which is one of the preceding cells of the current cell. The range of  $i$  depends on the quantity of preceding cells.

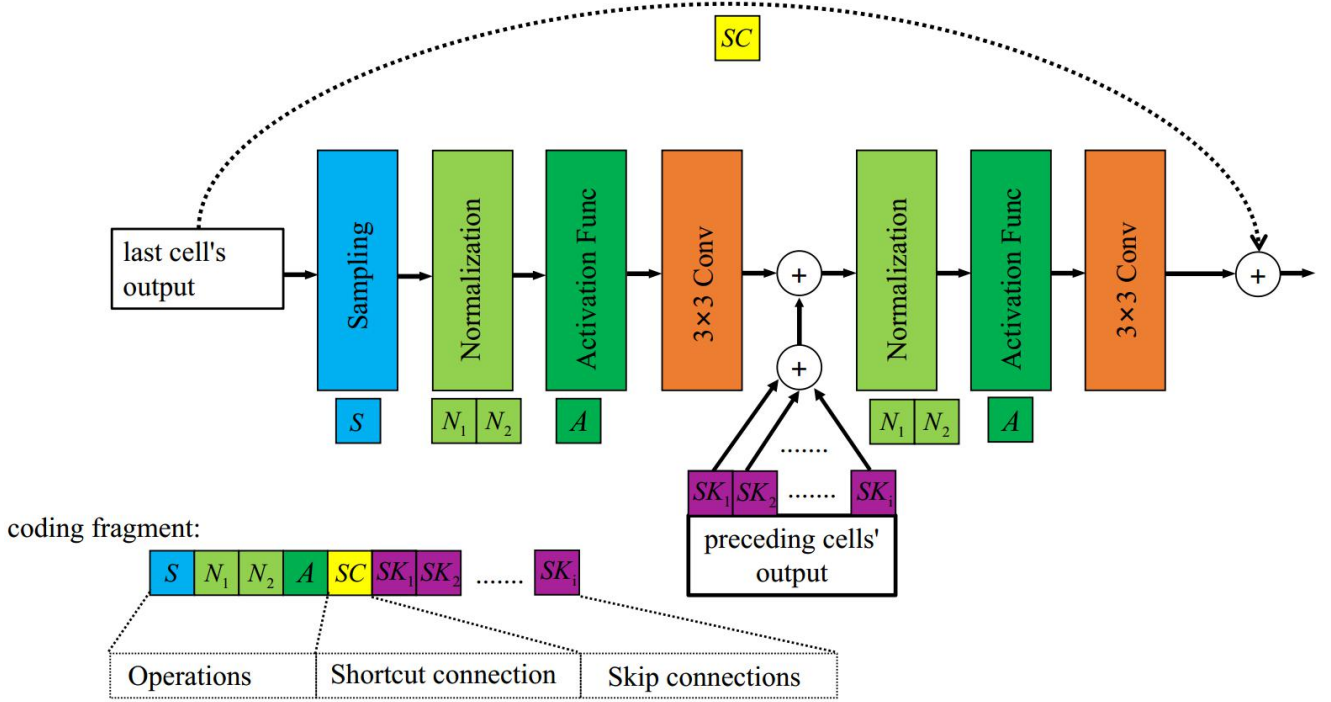


Figure 3. Example of genotype and phenotype. This is the cell encoding fragment and its corresponding phenotype. Different bits indicate different operation or connections. S, N, A, SC, SK represent sampling method, normalization method, activation function, shortcut connection, skip connection, respectively.

It should be noted that there aren't  $S$ ,  $SC$  and  $SK$  in the initial-conv cell. Each cell is represented by a fixed-length bit fragment, but their code lengths aren't the same because of different operations. Often the later cells will be with more bits of  $SK$ , since they can have more skip connections from preceding cells. The genotype of the whole neural network architecture is spliced by code fragments of different cells. In the process of searching architecture, it is to directly operate the genotype of network architecture.

### 3.3 Optimization Method

The encoding method of the architecture is introduced last section. We use the modified evolutionary strategy (ES) to optimize the architecture by operating on the genotype of the network architecture. The network architectures corresponding to individuals will be evaluated and assigned fitness during evolving. When evaluating the network architecture, the model needs to be trained from scratch with trainset. The process of optimizing the model is as follows:

- (1) Initialize  $\mu$  individuals as parent  $P$ , and train each model represented by  $P$  by assigning F1-score as fitness.
- (2) Generate  $\lambda$  off-springs  $C$  by random mutation from  $P$ .

- (3) Evaluate the architecture represented by  $C$  by training with gradient descent in parallel, and assign F1-score evaluated on test set as the fitness.
- (4) Put the  $\mu$  parents and  $\lambda$  off-springs together to get best  $\mu$  individuals, and then replace  $P$  with the best  $\mu$  individuals.
- (5) Return to step 2 until stop criteria are met.

In the above paper, we adopt the  $\mu + \lambda$  evolution strategy (with  $\mu = 9$ ,  $\lambda = 9$  in our experiment). When initializing the initial population, we do not use a completely random initialization method. In [36], an initialization method called Rich Initialization is introduced, and it has been proved to work better than random initialization. Inspired by this, we also adopt a similar initialization method which there will be a shortcut connection in all cells of the network architecture represented by the initial  $P$ , and different cells will be connected with all preceding cells. There is only mutation in the operation of evolution strategy. In our method, every individual in the population will mutate, and the mutation probability  $p$  of each bit is 0.1.

Using modified ES as optimization method is that the ES can evolve with a small number of individuals per generation so that the requirement for GPU quantity is more flexible, and neural architectures can evolve under our very limited computing resources. Another reason is that reinforcement learning as optimization method requires lots of random samplings of the network architectures and requires huge computing power to evaluate them. And differentiable neural architecture search is with high requirements for GPU memory. The modified ES which we adopt is able to compromise what is mentioned above.

## 4. Material

### 4.1 Loss function

Focal loss[18] is proposed to cope with the imbalance of positive and negative samples. When vanilla cross-entropy is used as the loss function for imbalanced classification, the model is more likely to be affected by negative samples and easy samples, which leads to the overall learning direction of the model deviating. As a result, the model fails to learn positive and hard samples correctly. Based on vanilla cross-entropy, Focal loss adds two parameters ( $\alpha$  and  $w$ ) to alleviate this problem.  $\alpha$  is used to adjust the weight of loss function for positive and negative samples, and  $w$  is used to adjust the weight of loss function for hard samples and easy samples. As in equation (1),  $y, \hat{y}, n, m$  denote ground truth, model prediction,  $n$ -th sample, total sample, respectively.

$$L = - \sum_{n=1}^m (\alpha y_n (1 - \hat{y}_n)^w \log \hat{y}_n + (1 - \alpha) (1 - y_n) \hat{y}_n^w \log (1 - \hat{y}_n)) \quad (1)$$

### 4.2 Dataset

In our work, we mainly use three public datasets: DRIVE[13], CHASE\_DB1[14], STARE[39]. An overview of these 3 publicly available datasets is provided in Table 2. Also, some examples of these 3 datasets are shown in Figure 4.

**Table 2. Overview of the adopted datasets in this paper**

Dataset	quantity	Resolution	Train-test split
DRIVE	40	$565 \times 584$	Official train-test split
STARE	20	$700 \times 605$	Leave-one-out split
CHASE_DB1	28	$999 \times 960$	First 20 for train, last 8 for test

The three public datasets contain the manual annotations of two experts, and we only take the annotations of the first expert as the ground truth. Unlike the patch-based methods, we use the original images without cropping as the input of the models. As well as, CHASE\_DB1 and STARE do not



have a predefined train-test split. In order to compare with other methods more fairly, we use the same train-test split as other papers [15][23][28].

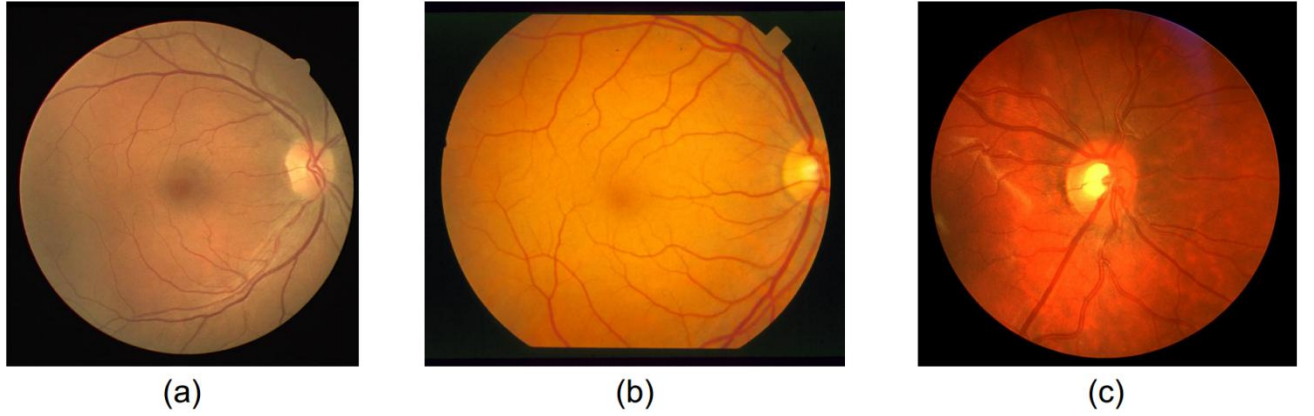


Figure 4. Examples of training images ( $H \times W$ ). (a): DRIVE ( $584 \times 565$ ); (b): STARE ( $700 \times 605$ ); (c): CHASE\_DB1 ( $960 \times 999$ )

### 4.3 Evaluation Metrics

RVS, a binary classification problem, is to predict whether the pixels of retina vessel images belong to vessel (positive) or non-vessel(negative).  $TP$ ,  $FP$ ,  $TN$ ,  $FN$  represent true positive, false positive, true negative, false negative, respectively. As shown in Table 3, there are the five metrics selected. These metrics are all based on  $TP$ ,  $FP$ ,  $TN$ ,  $FN$ . In our work, the global threshold  $\tau$  is set to 0.5 when calculating  $TP$ ,  $FP$ ,  $TN$ ,  $FN$ , except for  $AUROC$  which is calculated by different thresholds.

**Table 3. The evaluation metrics in our method**

Metric	Description
$ACC$ (accuracy)	$ACC = (TP + TN) / (TP + TN + FP + FN)$
$SE$ (sensitivity)	$SE = TP / (TP + FN)$
$SP$ (specificity)	$SP = TN / (TN + FP)$
$F1$ -score( $F1$ )	$F1 = (2 \times TP) / (2 \times TP + FP + FN)$ (2)
$AUROC$	Area Under the ROC curve.

### 4.4 Objective Function for Evolving

RVS is not only a dense prediction problem, but also an imbalanced classification problem. In a fundus image, the non-vessel area is more than 90%. Therefore, when comprehensively evaluating the model performance,  $ACC$  should not be adopted, and more comprehensive metrics, such as  $F1$ -score and  $AUROC$ , need to be considered. In the process of evolving network architecture, our work uses  $F1$ -score as fitness for this single-objective optimization problem, so the goal of optimization is to maximize Equation (2).

## 5. Experiments

### 5.1 Implement details

All the experiments are performed on a GPU server, which has four NVIDIA TITAN Xp GPU with 12GB memory each. During the evolution of the neural network architecture, each architecture in the evolution process needs to be evaluated. The evaluation method is to train the model by gradient descent with trainset, and then use the test set to evaluate the performance of the model and assign fitness to the corresponding individual. In the above training process, we use DRIVE dataset with a batch size of 2. At the same time, the optimizer we used is Lookahead[16] with Adam[17] as the base optimizer ( $\beta_1 = 0.9$ ,  $\beta_2 = 0.999$ ). The Lookahead optimizer is adopted default parameters, where  $\alpha =$



0.5,  $k = 6$ . Among them, the learning rate initialized during the training process is 0.001, and gradient is clipped with the L1 norm threshold of 0.1.

Aiming at the data imbalance of RVS, we used Focal loss[18] (The two parameters,  $w$  and  $\gamma$ , are set to 0.55 and 2.0, respectively). In this paper, all loss functions will use Focal loss by default if there is no special prompt, and the parameter settings are the same as above. During the evolution of the neural network architecture, the pixels of the images are normalized to the range of  $[-1,1]$ . We train each neural network model for 100 epochs, and take the F1-score calculated on the test set as the fitness of the corresponding individual in the evolution process.

Encoding representation of the neural network architecture have been introduced in previous section and each cell is with its corresponding fixed-length coding fragment. In our method, 54 bits are used to encode a neural network architecture. When using the  $\mu + \lambda$  evolution strategy to evolve the neural network architecture,  $\mu$  and  $\lambda$  are both set to 9, which means that the size of the population is 9. This setting is related to the number of GPUs. In the process of searching, 3 GPUs are used, and three neural network models are trained in parallel. At the same time, in order to maintain the efficiency of searching during evolution,  $\mu$  is also set to 9. The maximal number of explored individuals is  $9 \times 100 = 900$ . When training, F1-score after each epoch will be calculated. If the F1-score exceeds 20 epochs without increase, it is considered that the model no longer needs to continue training, and the training is terminated to save computing resources.

## 5.2 Results of architecture evolution

As shown in Table 4, the maximum (*Max*), minimum (*Min*), mean (*Avg*), median (*Med*), and standard deviation (*Std*) of fitness among all individuals in the corresponding generation during the evolution process. From the data in the Table 3, it can be seen that the *Max*, *Min*, *Avg* and *Med* of fitness in each generation are increasing generation by generation, and *Std* of fitness in each generation is continuously decreasing. This is very important, indicating that the individuals in the population are getting better and better during the evolution process.

**Table 4. F1 score on the DRIVE test set during evolving. The zero generation is the initial population.**

Gen	Max	Min	Avg	Med	Std
0	0.8120	0.7905	0.7995	0.7993	0.2483
3	0.8171	0.8063	0.8102	0.8104	0.0031
12	0.8179	0.8155	0.8167	0.8171	0.0007
17	0.8199	0.8171	0.8178	0.8175	0.0008
33	0.8208	0.8189	0.8194	0.8191	0.0005
49	0.8211	0.8197	0.8205	0.8206	0.0004
68	0.8214	0.8204	0.8208	0.8209	0.0003
87	0.8218	0.8209	0.8212	0.8211	0.0002
99	0.8218	0.8210	0.8212	0.8211	0.0002

Figure 5 mainly shows the changes in fitness maximum and minimum values in each generation of the population during the evolution. Because the evolution strategy (ES) used in this paper will only retain the top  $\mu = 9$  elite individuals in each generation as new parent population. Before the evolution to the 100<sup>th</sup> generation, the maximum and minimum values of fitness in the population last for more than 10 generations from 87<sup>th</sup> generation, so we stop the evolution in the 100<sup>th</sup> generation and take the optimal individual of the 100<sup>th</sup> generation as the output of the final result. As shown in Figure 6, it is the model architecture corresponding to optimal individual.

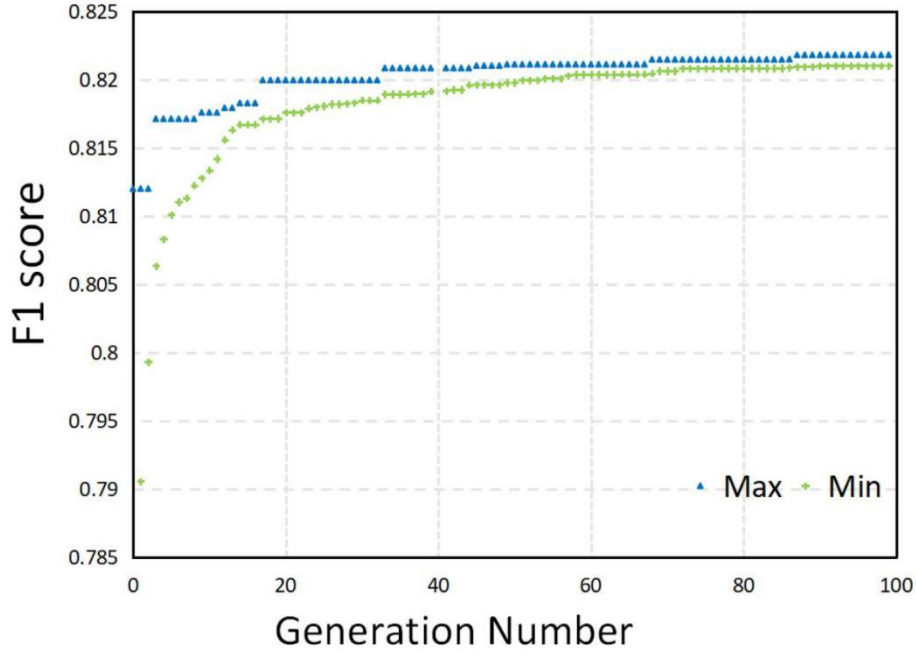


Figure 5. The maximum and minimum value of fitness over all individuals with respect to the generation number. The maximum and minimum values of fitness have the same development trend, and the D-value between them is getting smaller and smaller.

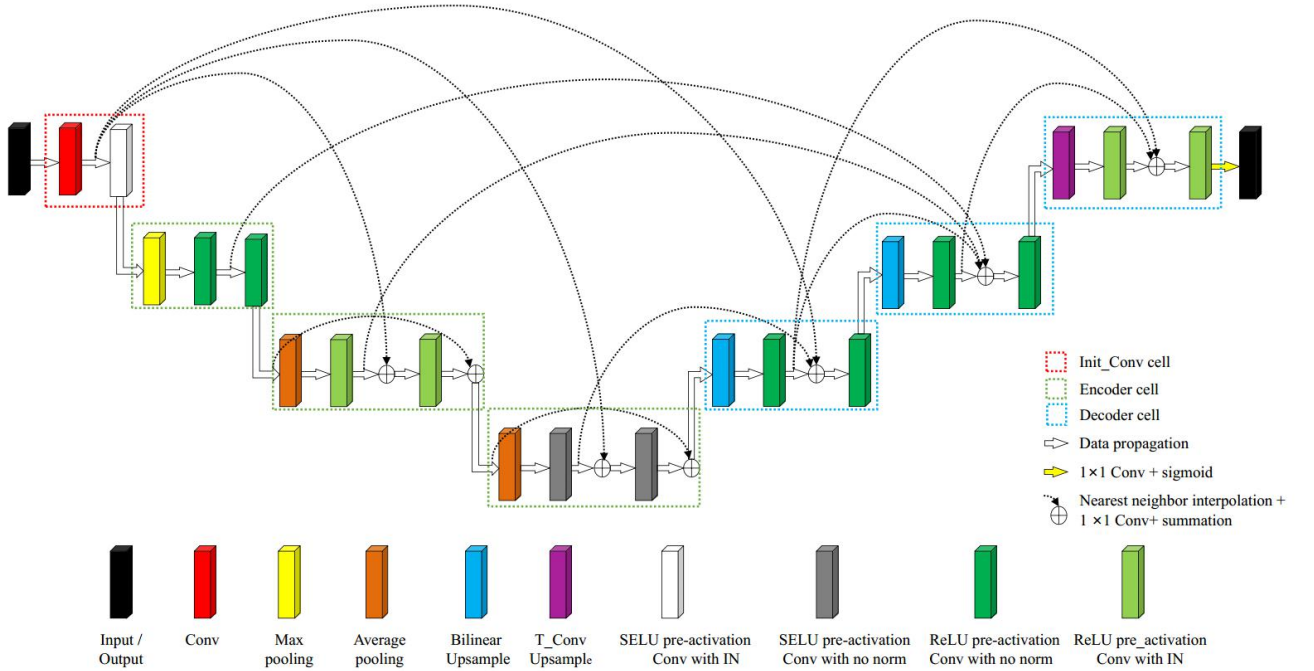


Figure 6. The searched model by our method on DRIVE dataset

### 5.3 Experiments with the searched model

We retrain final neural network model (searched on DRIVE dataset) from scratch on DRIVE, STARE and CHASE\_DB1. The parameter setting is basically the same as the setting when evaluating the model in the process of architecture evolution, including loss function, optimizer, etc. The main difference is that when retraining the model, data augmentation is carried out to avoid overfitting. For data augmentation, we used random horizontal and vertical flipping, and random rotation in the range of  $[-180^\circ, 180^\circ]$ . Unlike the patch-based method, we use the full image as the model input. Due to limitation of the GPU memory (12G), we set the batch size of the experiments on these three datasets

as 1 and train the models for 300 epochs.

### 5.3.1 Comparison with previous methods

Table 5, Table 6, Table 7 show the comparison between our method and the previous methods on the three datasets DRIVE, STARE, CHASE\_DB1, respectively. The metric data of the previous methods in these three tables are obtained from the original papers. These methods are representative methods based on deep learning and have achieved excellent results in retinal vessel segmentation. For DRIVE, our method achieves the best result in four of five metrics, only SP (specificity) is slightly lower than Fan et al.'s method [21] ( $0.9835 < 0.9849$ ). For STARE and CHASE\_DB1, our method achieves the best results in all five metrics compared to other methods with a considerable margin. Importantly, on three datasets, our method achieves the best results on two comprehensive metrics (F1 score and AUROC), which indicates the superiority of the searched model.

**Table 5. Comparison with previous methods on DRIVE dataset.**

Methods	Year	ACC	SE	SP	F1	AUROC
Vega <i>et al.</i> [20]	2015	0.9412	0.7444	0.9612	0.6884	N/A
Fan <i>et al.</i> [21]	2016	0.9614	0.7191	<b>0.9849</b>	N/A	N/A
Fan and Mo [22]	2016	0.9612	0.7814	0.9788	N/A	N/A
Liskowski <i>et al.</i> [23]	2016	0.9535	0.7811	0.9807	N/A	0.979
Li <i>et al.</i> [24]	2016	0.9527	0.7569	0.9816	N/A	0.9738
Orlando <i>et al.</i> [25]	2016	N/A	0.7897	0.9684	0.7857	N/A
Mo and Zhang [26]	2017	0.9521	0.7779	0.9780	N/A	0.9782
Xiao <i>et al.</i> [27]	2018	0.9655	0.7715	N/A	N/A	N/A
Alom <i>et al.</i> [28]	2019	0.9556	0.7792	0.9813	0.8171	0.9784
Jin <i>et al.</i> [31]	2019	0.9566	0.7963	0.9800	0.8237	0.9802
Bo Wang <i>et al.</i> [30]	2019	0.9567	0.7940	0.9816	0.8270	0.9772
Mou Lei <i>et al.</i> [40]	2019	0.9594	0.8126	0.9788	N/A	0.9796
Yicheng Wu <i>et al.</i> [29]	2019	0.9578	0.8038	0.9802	N/A	0.9821
The Proposed Method	2020	<b>0.9702</b>	<b>0.8341</b>	0.9835	<b>0.8297</b>	<b>0.9882</b>

**Table 6. Comparison with previous methods on STARE dataset.**

Methods	Year	ACC	SE	SP	F1	AUROC
Vega <i>et al.</i> [20]	2015	0.9483	0.7019	0.9671	0.6614	N/A
Fan <i>et al.</i> [21]	2016	0.9588	0.6996	0.9787	N/A	N/A
Fan and Mo [22]	2016	0.9654	0.7834	0.9799	N/A	N/A
Liskowski <i>et al.</i> [23]	2016	0.9729	0.8554	0.9862	N/A	0.9928
Li <i>et al.</i> [24]	2016	0.9628	0.7726	0.9844	N/A	0.9879
Orlando <i>et al.</i> [25]	2017	N/A	0.7680	0.9738	0.7644	N/A
Mo and Zhang [26]	2018	0.9674	0.8147	0.9844	N/A	0.9885
Xiao <i>et al.</i> [27]	2019	0.9693	0.7469	N/A	N/A	N/A
Alom <i>et al.</i> [28]	2019	0.9712	0.8292	0.9862	0.8475	0.9914
Jin <i>et al.</i> [31]	2019	0.9641	0.7595	0.9878	0.8143	0.9832
The Proposed Method	2020	<b>0.9786</b>	<b>0.8635</b>	<b>0.9881</b>	<b>0.8583</b>	<b>0.9937</b>

**Table 7. Comparison with previous methods on CHASE\_DB1 dataset.**

Methods	Year	ACC	SE	SP	F1	AUROC
Fan and Mo [22]	2016	0.9573	0.7656	0.9704	N/A	N/A
Liskowski <i>et al.</i> [23]	2016	0.9628	0.7816	0.9836	N/A	0.9823
Li <i>et al.</i> [24]	2016	0.9527	0.7569	0.9816	N/A	0.9738
Orlando <i>et al.</i> [25]	2016	N/A	0.7277	0.9712	0.7332	N/A
Mo and Zhang [26]	2017	0.9581	0.7661	0.9793	N/A	0.9812
Alom <i>et al.</i> [28]	2019	0.9634	0.7756	0.9820	0.7928	0.9815
Jin <i>et al.</i> [31]	2019	0.9610	0.8155	0.9752	0.7883	0.9804
Bo Wang <i>et al.</i> [30]	2019	0.9661	0.8074	0.9821	0.8037	0.9812
Yicheng Wu <i>et al.</i> [29]	2019	0.9661	0.8132	0.9814	N/A	0.9860
The Proposed Method	2020	<b>0.9759</b>	<b>0.8546</b>	<b>0.9839</b>	<b>0.8170</b>	<b>0.9909</b>

### 5.3.2 Comparison with representative models

Our method is with certain advantages over previous methods, but this comparison is not very rigorous, because many parameters may be different (e.g. loss function, optimizer, batch size, etc.). The results of the compared methods may be obtained under different and best possible parameters settings. Therefore, we only change the model architecture and perform comparison experiments under the same parameter setting. We compare the searched model with original U-Net [2] and Attention U-Net [19] (variant of original U-Net) in this paper.

As Table 7 shows, SP for Searched model, U-Net and Attention U-Net is 0.9835/0.9841/0.9841 on DRIVE, 0.9835/0.9861/0.9870 on CHASE\_DB1 and 0.9881/0.9895/0.9893, respectively. ACC for Searched model, U-Net and Attention U-Net is 0.9759/0.9762/0.9764 on CHASE\_DB1. The above mentioned is the all cases that the metrics of the searched model is slightly lower than U-Net and Attention U-Net but still comparable, and due to the data imbalance of RVS, ACC and SP cannot comprehensively and accurately evaluate the performances of the models. More importantly, the searched model achieves better results than U-Net and Attention U-Net in other comprehensive metrics, such as F1 score and AUROC.

What's more, we use ROC curves in Figure 7 and PR curves in Figure 8 to evaluate the models. The larger area under these two curves directly reflects the better performance of the model. For the ROC curve, the closer it is to the upper left corner, the larger the area under the curve, while for the PR curve, the closer it is to the upper right corner, the larger the area under the curve. It can be known from the figures that, whether it is ROC curves or PR curves, the searched model has the largest area under the curves among three models.

We also present some example results in Figure 9. The blue pixels in figures of the results indicate false negative, which is the vessel region not detected. As we can see, the searched model detects vessels more accurately than U-Net and Attention U-Net, no matter the overall view or the local magnified view. One of the most obvious is that the results of the searched model are with less blue pixels. U-Net and Attention U-Net show their limitations on extracting complicated structural features, while the searched model can extract these indistinct and detailed features better. The searched model still performs well on segmenting densely intersected vessels and tiny vessels. With advantages of architecture, the searched model is able to provide desirable segmentation results.

**Table 8. Comparison with U-Net and Attention U-Net on three datasets**

Dataset	Models	ACC	SE	SP	F1	AUROC
DRIVE	U-Net	0.9696	0.8218	<b>0.9841</b>	0.8249	0.9872
	Attention U-Net	0.9697	0.8229	<b>0.9841</b>	0.8250	0.9875
	Searched model	<b>0.9702</b>	<b>0.8341</b>	0.9835	<b>0.8297</b>	<b>0.9882</b>
CHASE_DB1	U-Net	<b>0.9764</b>	0.8180	<b>0.9870</b>	0.8137	0.9896
	Attention U-Net	0.9762	0.8295	0.9861	0.8146	0.9891
	Searched model	0.9759	<b>0.8546</b>	0.9839	<b>0.8170</b>	<b>0.9909</b>
STARE	U-Net	0.9750	0.7900	0.9893	0.8139	0.9884
	Attention U-Net	0.9754	0.7918	<b>0.9895</b>	0.8180	0.9868
	Searched model	<b>0.9786</b>	<b>0.8635</b>	0.9881	<b>0.8583</b>	<b>0.9937</b>

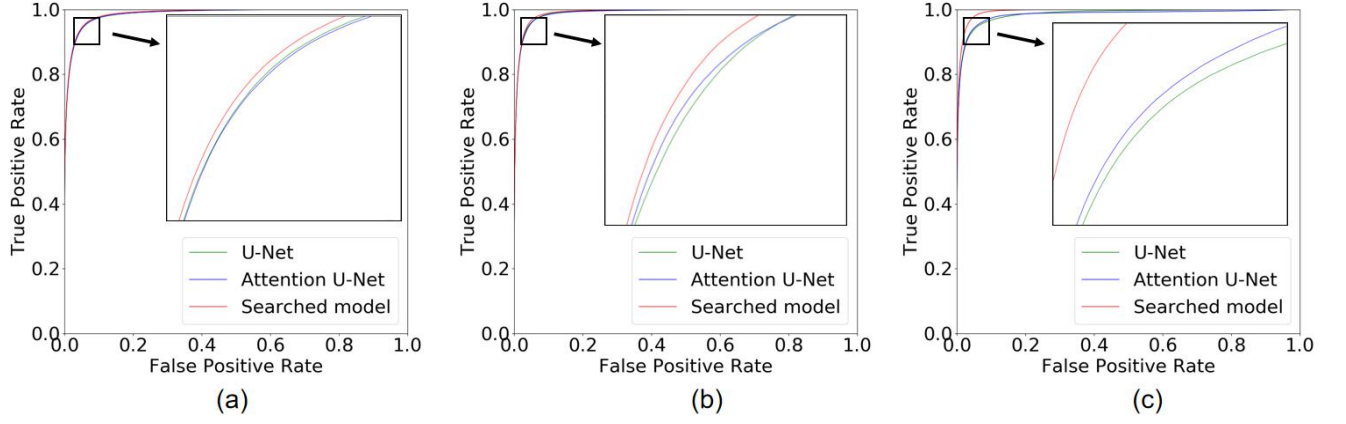


Figure 7. ROC Curves on three datasets. (a) DRIVE. (b) CHASE\_DB1. (c) STARE.

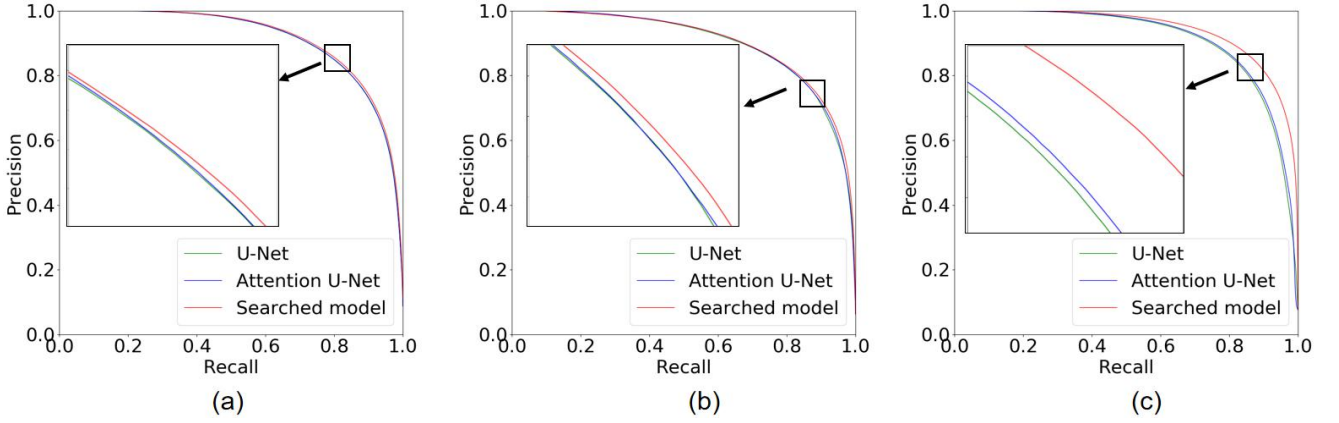


Figure 8. PR Curves on three datasets. (a) DRIVE. (b) CHASE\_DB1. (c) STARE.



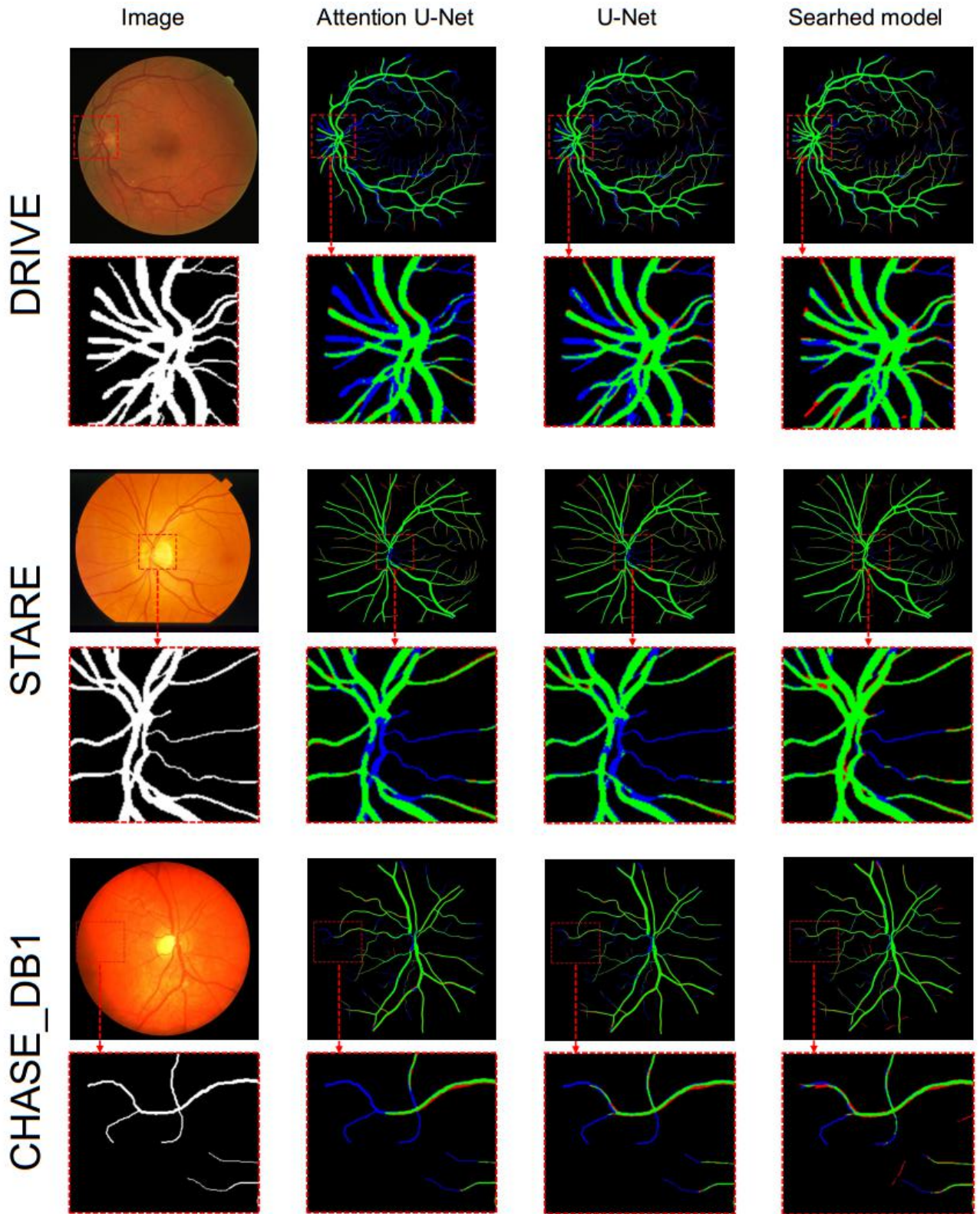


Figure 9. Visualization of the segmentation results on DRIVE, SATRE, and CHASE\_DB1 datasets. Green pixel indicates true positive, red pixel indicates false positive and blue pixel indicates false negative.

### 5.3.3 Cross-training evaluation

We access the scalability and robustness of the models by cross-training between the three datasets. The collection ways of DRIVE, STARE, and CHASE\_DB1 are different. The results of cross-training can be used to judge the adaptability of the models when the fundus images are from different sources. The cross-training results of the three models (the searched model, U-Net and Attention U-net) are

presented in Table 9. Compared to training and testing in a single dataset, the performances of the three models are all degraded, but the searched model is still most effective than the other two models, and it would not cause a sharp deterioration in performance. After cross-training, the advantages of the searched model are more prominent because the metric gap between three models is more obvious. One of the most obvious is that when using STARE as the test set and DRIVE as the training set, the F1 score and AUROC of the searched model, U-Net and Attention U-Net are 0.5816/0.5646/ 0.7905 and 0.9349/0.9497/0.9829, respectively. When using CHASE\_DB1 as the training set, the F1 score and AUROC obtained by the searched model, U-Net and Attention U-Net on STARE are 0.6377 / 0.6142 / 0.7050 and 0.9505 / 0.9203 / 0.9657, respectively. When CHASE\_DB1 is used as the test set, a similar situation occurs, and this situation is that U-Net and Attention U-Net perform very poorly and are with large performance deterioration. A possible explanation for situation of STARE is that STARE is a more complicated than the other datasets[31][41]. We consider that the situation of CHASE\_DB1 may be the same reason as STARE. But even in these cases, the searched model can still obtain stable performance, which indicates that the searched model is with considerable scalability and robustness. This also proves that the searched model is more reliable and with potential for clinical disease diagnosis.

**Table 9. Comparisons of the cross-training evaluation.**

Dataset	Models/Methods	ACC	SE	SP	F1	AUROC
DRIVE (trained on STARE)	U-Net	0.9647	0.7303	0.9874	0.7823	0.9749
	Attention U-Net	0.9663	0.7156	<b>0.9906</b>	0.7868	0.9794
	Searched model	<b>0.9672</b>	<b>0.7376</b>	0.9896	<b>0.7966</b>	<b>0.9819</b>
DRIVE (trained on CHASE_DB1)	U-Net	0.9565	0.6064	0.9903	0.7063	0.9568
	Attention U-Net	0.9565	0.5665	<b>0.9941</b>	0.6922	<b>0.9592</b>
	Searched model	<b>0.9578</b>	<b>0.6637</b>	0.9863	<b>0.7327</b>	0.9587
STARE (trained on DRIVE)	U-Net	0.9487	0.5942	0.9755	0.5816	0.9349
	Attention U-Net	0.9513	0.5359	0.9831	0.5646	0.9497
	Searched model	<b>0.9684</b>	<b>0.8065</b>	0.9814	<b>0.7905</b>	<b>0.9829</b>
STARE (trained on CHASE_DB1)	U-Net	0.9562	0.6003	0.9839	0.6377	0.9505
	Attention U-Net	0.9553	0.5676	<b>0.9854</b>	0.6142	0.9203
	Searched model	<b>0.9567</b>	<b>0.7517</b>	0.9724	<b>0.7050</b>	<b>0.9657</b>
CHASE_DB1 (trained on DRIVE)	U-Net	0.9278	0.4704	0.9633	0.4591	0.9240
	Attention U-Net	0.9407	0.3641	<b>0.9865</b>	0.4421	0.9110
	Searched model	<b>0.9685</b>	<b>0.8241</b>	0.9801	<b>0.7940</b>	<b>0.9829</b>
CHASE_DB1 (trained on STARE)	U-Net	0.9463	0.5690	0.9745	0.5926	0.9355
	Attention U-Net	0.9501	0.6070	<b>0.9756</b>	0.6248	0.9304
	Searched model	<b>0.9567</b>	<b>0.7517</b>	0.9724	<b>0.7050</b>	<b>0.9567</b>

## 6. Conclusion

In this paper, neural architecture search (NAS) is applied to retinal vessel segmentation. Based on the proposed specific search space, we adopt the modified evolutionary strategy to search the macro-architecture of the neural network. Compared to other models, the searched model is able to capture more features about the complicated vascular tree from fundus image and provide better segmentation result with fewer parameters. Furthermore, the searched model is with considerable scalability, which indicates the application potential in clinical diagnosis. We expect that the searched



model or architecture search method in our work can also successfully extended to related tasks, such as pavement crack segmentation or other medical image segmentation, even semantic segmentation of urban scenes.

## References

- [1] Long, Jonathan, Evan Shelhamer, and Trevor Darrell. "Fully convolutional networks for semantic segmentation." *Proceedings of the IEEE conference on computer vision and pattern recognition*. 2015.
- [2] Ronneberger, Olaf, Philipp Fischer, and Thomas Brox. "U-net: Convolutional networks for biomedical image segmentation." *International Conference on Medical image computing and computer-assisted intervention*. Springer, Cham, 2015.
- [3] Gong, Xinyu, et al. "AutoGAN: Neural Architecture Search for Generative Adversarial Networks." *Proceedings of the IEEE International Conference on Computer Vision*. 2019.
- [4] Liu, Chenxi, et al. "Auto-deeplab: Hierarchical neural architecture search for semantic image segmentation." *Proceedings of the IEEE Conference on Computer Vision and Pattern Recognition*. 2019.
- [5] Miikkulainen, Risto, et al. "Evolving deep neural networks." *Artificial Intelligence in the Age of Neural Networks and Brain Computing*. Academic Press, 2019. 293-312.
- [6] Simonyan, Karen, and Andrew Zisserman. "Very deep convolutional networks for large-scale image recognition." *ICLR*, 2015.
- [7] Nair, Vinod, and Geoffrey E. Hinton. "Rectified linear units improve restricted boltzmann machines." *Proceedings of the 27th international conference on machine learning (ICML-10)*. 2010.
- [8] Klambauer, Günter, et al. "Self-normalizing neural networks." *Advances in neural information processing systems*. 2017.
- [9] Ioffe, Sergey, and Christian Szegedy. "Batch normalization: Accelerating deep network training by reducing internal covariate shift." *arXiv preprint arXiv:1502.03167* (2015).
- [10] Ulyanov, Dmitry, Andrea Vedaldi, and Victor Lempitsky. "Instance normalization: The missing ingredient for fast stylization." *arXiv preprint arXiv:1607.08022* (2016).
- [11] Lu, Zhichao, et al. "NSGA-Net: neural architecture search using multi-objective genetic algorithm." *Proceedings of the Genetic and Evolutionary Computation Conference*. ACM, 2019.
- [12] Xie, Lingxi, and Alan Yuille. "Genetic cnn." *Proceedings of the IEEE International Conference on Computer Vision*. 2017.
- [13] Staal, Joes, et al. "Ridge-based vessel segmentation in color images of the retina." *IEEE transactions on medical imaging* 23.4 (2004): 501-509.
- [14] Fraz, Muhammad Moazam, et al. "An ensemble classification-based approach applied to retinal blood vessel segmentation." *IEEE Transactions on Biomedical Engineering* 59.9 (2012): 2538-2548.
- [15] Orlando, José Ignacio, Elena Prokofyeva, and Matthew B. Blaschko. "A discriminatively trained fully connected conditional random field model for blood vessel segmentation in fundus images." *IEEE transactions on Biomedical Engineering* 64.1 (2016): 16-27.
- [16] Zhang, Michael, et al. "Lookahead Optimizer: k steps forward, 1 step back." *Advances in Neural Information Processing Systems*. 2019.
- [17] Kingma, Diederik P., and J. Ba. "Adam: A Method for Stochastic Optimization." *Computer Science* (2014).
- [18] Lin, Tsung-Yi, et al. "Focal loss for dense object detection." *Proceedings of the IEEE international conference on computer vision*. 2017.
- [19] Oktay, Ozan, et al. "Attention u-net: Learning where to look for the pancreas." *MIDL*, 2018.
- [20] Vega, Roberto, et al. "Retinal vessel extraction using lattice neural networks with dendritic processing." *Computers in biology and medicine* 58 (2015): 20-30.
- [21] Fan, Zhun, et al. "Automated blood vessel segmentation in fundus image based on integral channel features and

random forests." 2016 12th World Congress on Intelligent Control and Automation (WCICA). IEEE, 2016.

[22] Fan, Zhun, and Jia-Jie Mo. "Automated blood vessel segmentation based on de-noising auto-encoder and neural network." 2016 International Conference on Machine Learning and Cybernetics (ICMLC). Vol. 2. IEEE, 2016.

[23] Liskowski, Paweł, and Krzysztof Krawiec. "Segmenting retinal blood vessels with deep neural networks." *IEEE transactions on medical imaging* 35.11 (2016): 2369-2380.

[24] Li, Qiaoliang, et al. "A cross-modality learning approach for vessel segmentation in retinal images." *IEEE transactions on medical imaging* 35.1 (2015): 109-118.

[25] Orlando, José Ignacio, Elena Prokofyeva, and Matthew B. Blaschko. "A discriminatively trained fully connected conditional random field model for blood vessel segmentation in fundus images." *IEEE transactions on Biomedical Engineering* 64.1 (2016): 16-27.

[26] Mo, Juan, and Lei Zhang. "Multi-level deep supervised networks for retinal vessel segmentation." *International journal of computer assisted radiology and surgery* 12.12 (2017): 2181-2193.

[27] Xiao, Xiao, et al. "Weighted Res-UNet for High-Quality Retina Vessel Segmentation." 2018 9th International Conference on Information Technology in Medicine and Education (ITME). IEEE, 2018.

[28] Alom, Md Zahangir, et al. "Recurrent residual U-Net for medical image segmentation." *Journal of Medical Imaging* 6.1 (2019): 014006.

[29] Wu, Yicheng, et al. "Vessel-Net: retinal vessel segmentation under multi-path supervision." *International Conference on Medical Image Computing and Computer-Assisted Intervention*. Springer, Cham, 2019.

[30] Wang, Bo, Shuang Qiu, and Huiguang He. "Dual Encoding U-Net for Retinal Vessel Segmentation." *International Conference on Medical Image Computing and Computer-Assisted Intervention*. Springer, Cham, 2019.

[31] Jin, Qiangguo, et al. "DUNet: A deformable network for retinal vessel segmentation." *Knowledge-Based Systems* 178 (2019): 149-162.

[32] Fraz, Muhammad Moazam, et al. "Delineation of blood vessels in pediatric retinal images using decision trees-based ensemble classification." *International journal of computer assisted radiology and surgery* 9.5 (2014): 795-811.

[33] Fraz, Muhammad Moazam, et al. "An ensemble classification-based approach applied to retinal blood vessel segmentation." *IEEE Transactions on Biomedical Engineering* 59.9 (2012): 2538-2548.

[34] Zhao, He, et al. "Supervised segmentation of un-annotated retinal fundus images by synthesis." *IEEE transactions on medical imaging* 38.1 (2018): 46-56.

[35] Meyer, Maria Ines, et al. "A deep neural network for vessel segmentation of scanning laser ophthalmoscopy images." *International Conference Image Analysis and Recognition*. Springer, Cham, 2017.

[36] Suganuma, Masanori, Shinichi Shirakawa, and Tomoharu Nagao. "A genetic programming approach to designing convolutional neural network architectures." *Proceedings of the Genetic and Evolutionary Computation Conference*. ACM, 2017.

[37] He, Kaiming, et al. "Deep residual learning for image recognition." *Proceedings of the IEEE conference on computer vision and pattern recognition*. 2016.

[38] Huang, Gao, et al. "Densely connected convolutional networks." *Proceedings of the IEEE conference on computer vision and pattern recognition*. 2017.

[39] Hoover, A. D. , V. Kouznetsova , and M. Goldbaum . "Locating Blood Vessels in Retinal Images by Piecewise Threshold Probing of a Matched Filter Response." *IEEE Transactions on Medical Imaging* 19.3(2000):203-210.

[40] Mou, Lei, et al. "Dense Dilated Network with Probability Regularized Walk for Vessel Detection." *IEEE transactions on medical imaging* (2019).

[41] Yan, Zengqiang, Xin Yang, and Kwang-Ting Tim Cheng. "A three-stage deep learning model for accurate retinal vessel segmentation." *IEEE journal of biomedical and health informatics* (2018).

[42] Bowen Baker, Otkrist Gupta, Nikhil Naik, and Ramesh Raskar. *Designing neural network architectures using reinforcement learning*. ICLR, 2017.

- [43] Barret Zoph and Quoc V Le. Neural architecture search with reinforcement learning. ICLR, 2017.
- [44] Barret Zoph, Vijay Vasudevan, Jonathon Shlens, and Quoc V Le. Learning transferable architectures for scalable image recognition. In CVPR, pages 8697–8710, 2018.
- [45] Hanxiao Liu, Karen Simonyan, and Yiming Yang. Darts: Differentiable architecture search. ICLR, 2019.
- [46] Andrew Brock, Theodore Lim, James M Ritchie, and Nick Weston. Smash: one-shot model architecture search through hypernetworks. ICLR, 2018.
- [47] Ghiasi, Golnaz, Tsung-Yi Lin, and Quoc V. Le. "Nas-fpn: Learning scalable feature pyramid architecture for object detection." Proceedings of the IEEE Conference on Computer Vision and Pattern Recognition. 2019.
- [48] Xu, Hang, et al. "Auto-fpn: Automatic network architecture adaptation for object detection beyond classification." Proceedings of the IEEE International Conference on Computer Vision. 2019.
- [49] Zhuotun Zhu, Chenxi Liu, Dong Yang, Alan Yuille, and Daguang Xu. V-nas: Neural architecture search for volumetric medical image segmentation. 3DV, 2019.
- [50] Dong Yang, Holger Roth, Ziyue Xu, Fausto Milletari, Ling Zhang, and Daguang Xu. Searching learning strategy with reinforcement learning for 3d medical image segmentation. In MICCAI, pages 3–11. Springer, 2019.
- [51] Aliasghar Mortazi and Ulas Bagci. Automatically designing cnn architectures for medical image segmentation. In MLMI, pages 98–106. Springer, 2018.
- [52] Yu Weng, Tianbao Zhou, Yujie Li, and Xiaoyu Qiu. Nas-unet: Neural architecture search for medical image segmentation. IEEE Access, 7:44247–44257, 2019.
- [53] Sungwoong Kim, Ildoo Kim, Sungbin Lim, Woonhyuk Baek, Chiheon Kim, Hyungjoo Cho, Boogeon Yoon, and Taesup Kim. Scalable neural architecture search for 3d medical image segmentation. arXiv preprint arXiv:1906.05956, 2019.
- [54] Laibacher, Tim, Tillman Weyde, and Sepehr Jalali. "M2U-Net: Effective and Efficient Retinal Vessel Segmentation for Real-World Applications." Proceedings of the IEEE Conference on Computer Vision and Pattern Recognition Workshops. 2019.
- [55] Yan, Zengqiang, Xin Yang, and Kwang-Ting Cheng. "Joint segment-level and pixel-wise losses for deep learning based retinal vessel segmentation." IEEE Transactions on Biomedical Engineering 65.9 (2018): 1912-1923.
- [56] Chatziralli, Irini P., et al. "The value of fundoscopy in general practice." The open ophthalmology journal 6 (2012): 4.
- [57] Fraz, M. M. , et al. "Blood vessel segmentation methodologies in retinal images – A survey." Computer Methods and Programs in Biomedicine 108.1(2012):407-433.
- [58] Vostatek, Pavel , et al. "Performance Comparison of Publicly Available Retinal Blood Vessel Segmentation Methods." Computerized Medical Imaging and Graphics 55(2016):2-12.
- [59] Ortega, Marcos , et al. "Personal verification based on extraction and characterization of retinal feature points." Journal of Visual Languages & Computing 20.2(2009):80-90.
- [60] Simon and I. Goldstein. A new scientific method of identification. New York State Journal of Medicine, 35(18):901–906, Sept. 1935
- [61] Sandler, Mark, et al. "Mobilenetv2: Inverted residuals and linear bottlenecks." Proceedings of the IEEE Conference on Computer Vision and Pattern Recognition. 2018.